Chemical and electronic properties of Al/[vicinal GaAs(100)] and Au/[vicinal GaAs(100)] interfaces

S. Chang, I. M. Vitomirov, and L. J. Brillson
Xerox Webster Research Center, 900 Phillips Road, Webster, New York 14580

C. Mailhiot
Lawrence Livermore National Laboratory, University of California, Livermore, California 94550

D. F. Rioux
Department of Physics, University of Wisconsin, Madison, Wisconsin 53706

Y. J. Kime
Department of Physics, Syracuse University, Syracuse, New York 13210

P. D. Kirchner, G. D. Pettit, and J. M. Woodall
IBM Thomas J. Watson Research Center, Yorktown Heights, New York 10598
(Received 15 August 1991)

Soft-x-ray photoemission studies of Al and Au on molecular-beam epitaxially grown GaAs(100) vicinal surfaces at low temperature demonstrate orientation-dependent interface electronic properties and chemistry. Misorientation of the substrate introduces both electrically and chemically active sites. With increasing misorientation-induced step-site density, the Fermi level at the Al/GaAs(100) interface moves toward the midgap. For the Au/GaAs(100) interface, substrate misorientation has only a minor effect on the electronic barrier height. The chemically active sites modify the extent of interface chemistry. A self-consistent electrostatic calculation of the misorientation-dependent barrier height for Al interfaces indicates a nearly one-to-one correlation between interface states and step-induced bonding sites. These results emphasize the importance of an atomic-scale interface bonding structure in the Schottky-barrier formation.

I. INTRODUCTION

The formation of an electrostatic potential barrier due to charge transfer at a metal-semiconductor contact remains controversial despite more than 50 years of extensive study.[1-4] In Schottky's early phenomenological description, the barrier height should equal the difference between the work function of the metal and the electron affinity of the semiconductor.[5] However, experimental results for many metal-semiconductor interfaces have revealed the barrier height to be insensitive to this difference.[1-4] This insensitivity has hampered researchers' ability to tailor contact electronic barrier properties and consequently has limited semiconductor device applications. For example, barrier measurements have revealed that the Fermi level (E_F) at metal-GaAs contacts stabilizes near midgap in a narrow range of $\sim 0.2-0.3$ eV.[1-4] This "pinning" makes both Ohmic and rectifying contacts difficult to obtain for this otherwise high-performance device material.

Numerous physical models have been proposed to explain E_F "pinning" at metal-semiconductor interfaces. Leading interpretations include the following. (1) The overlayer metal wave function tunnels into the semiconductor gap, which creates a continuum distribution of localized gap states. A calculated charge-neutrality level determines the position of E_F.[6,7] (2) Native defects or defects caused by adatom condensation produce discrete electronic states and stabilize the E_F.[8,9] (3) Interface chemical and structural modifications, such as atomic interdiffusion, formation of new compounds, and the metal-semiconductor bonding produce discrete gap states which stabilize the E_F.[1,10] These states are interface specific. (4) The effective work function of interface phases resulting from a reaction determines the E_F.[10] Additional models involve variations or combinations of the above.

Recently, it has been demonstrated that near-ideal Schottky contacts can be grown under specific conditions: metalization of molecular-beam epitaxy (MBE) GaAs(100) surfaces at low temperature (90 K).[11,12] Studies of electronic gap states with cathodoluminescence and photoluminescence spectroscopies indicate significantly less bulk defect states in MBE- than in melt-grown semiconductors [e.g., GaAs (Refs. 11 and 13) and CdTe (Ref. 14)]. In addition, luminescence measurements show that the metalization of semiconductor surfaces induces a significantly higher density of gap states on melt-grown semiconductors than on MBE-grown semiconductors.[13-15] These developments are direct results of the increasing sophistication of semiconductor and surface processing. The attainment of nearly "unpinned" Schottky barriers suggests a need for reevaluation of models which contain pinning as an intrinsic feature of

the metal-semiconductor interface.

Because of the wide range of E_F movement now possible at these interfaces, one can study the influence of surface structural modifications on the interface states and barrier heights. In this work, we examine the dependence of Schottky-barrier heights and interface chemistry on the misorientation of GaAs(100) vicinal surfaces. Here we provide a full description of experiments to investigate (1) the chemical activity associated with the nature and the density of misorientation-induced structural sites, (2) the formation of electronic states associated with these nucleation sites, and (3) the role of these sites in Schottky-barrier formation. Finally, we discuss the implications of these results from the models of Schottky-barrier formation already mentioned.

II. EXPERIMENTAL PROCEDURES

We carried out soft-x-ray photoemission measurements (SXPS) at the University of Wisconsin–Madison using the Aladdin electron storage ring. The monochromatized synchrotron radiation from the Mark II and Mark V grasshopper monochromators photoexcite electrons, which were energy resolved through a double-pass cylindrical mirror analyzer. We collected energy distribution curves (EDC's) at incident photon energies of 80 and 40 eV for the Ga 3*d* core level and at incident photon energies of 100 and 60 eV for the As 3*d* core level to probe the interface at two different depths. Typical electron escape depths are ~4–6 and ~8–10 Å for the higher and lower photon energies selected.[16] We also examined the Al 2*p* core level at 120 eV and the valence band (VB) at 47-eV photon energies. The overlapping of the reacted and substrate core-level emissions can be deconvolved with a nonlinear least-squares curve fit. The band bending is equal to the rigid shift of the substrate components of the 3*d* core levels. The Ga 3*d* and As 3*d* components associated with the interface disruption as well as core-level attenuation profiles were used to examine the interface chemistry and morphology. The linear extrapolation of the VB edge to an onset of photoemission determines the initial value of E_F referenced to the VB maximum (E_V). The evolution of the VB edge into a metallic density of states and the appearance of an asymmetric line shape in the Al 2*p* core emission due to plasmon losses show the surface metallization. The VB shape was also used to monitor adatom-substrate interaction and surface contamination. The overall monochromator-spectrometer resolution of 0.25–0.3 eV was determined from the width of the Fermi edge of a 200-Å Au film deposited onto a thermally cleaned GaAs(100) surface. All EDC's collected were normalized to the throughput of the monochromator, measured by a nickel mesh located at the exit of the monochromator.

We also performed cathodoluminescence spectroscopy (CLS) in conjunction with SXPS for Al and Au on GaAs(100) and GaAs(100)2°→[110]. A grazing incident electron beam with 1.5-kV electron energy and 6-μA beam current (measured at the substrate) generated electron-hole pairs. A CaF_2 lens positioned *in situ* focuses the luminescence light through a sapphire window onto the entrance slit of a Leiss single-pass monochromator with flint-glass prisms. The light was detected with a liquid-nitrogen-cooled Ge detector with a cutoff energy at 0.7 eV. The full width at half maximum of the band-to-band transition was ≤ 50 meV, decreasing at lower photon energies. The measured optical system response provided a normalization of the spectrally resolved luminescence from the specimen.

GaAs specimens were 7500-Å-thick, *n*-type ($5\times10^{16}/cm^3$, Si) MBE grown on 2-in. melt-grown GaAs wafers. We used the following vicinal substrates: 2° and 4°→[110], 2° and 4°→[111] with Ga dangling bonds perpendicular to steps (*A* type), and 1°, 2° and 4°→[111] with As dangling bonds perpendicular to steps (*B* type), with angular precision of ±0.1°. The vicinal surface 2°→$[111]_A$ and $[111]_B$, 4°→[110], $[111]_A$, and $[111]_B$ were grown on both semi-insulating substrates and degenerately doped substrates. All wafers were coated with a 1–2000-Å As layer before removal from the MBE system to prevent atmospheric contamination. They were then stored in N_2 or vacuum for several days until the time of the experiments. Tantalum (Ta) foils mounted onto oxygen-free Cu specimen holders provided heating for the specimen. For specimens grown on highly doped substrates, an indium back contact was used to improve electrical and thermal conduction. For specimens grown on semi-insulating substrates, Au was evaporated onto the sides of the specimen's front surface. In this case, the Ta clips used for mounting and heating also provided the grounding for the specimen.

The As cap layer was removed by thermal desorption in the analysis chamber.[13] An infrared pyrometer (Optitherm) measured the specimen temperature through a sapphire window. During the desorption of bulk As (400 °C), the pressure in our chamber remained steady at $\sim1\times10^{-10}$ Torr (base pressure $\sim8\times10^{-11}$ Torr) until ~340 °C where it rose to a pressure between 5×10^{-8} and 2×0^{-7} Torr. The pressure recovered to $\leq5\times10^{-9}$ Torr when substrate temperature reached ~380 °C. The specimen surface displayed a "defogging" phenomenon visually observable during this period: changing from a cloudy gray to a mirrorlike finish. The desorption of more "tightly bound" As (Ref. 13) was proceeded by consecutive ramped heatings starting at 550 °C with 5 °C–10 °C increment for each additional ramp. Here, the pressure rose gradually to between 8×10^{-10} and 2×10^{-9} Torr. Any drastic increase in pressure was observed in conjunction with GaAs decomposition. During the desorption of surface As, the surface was checked spectroscopically before each additional heating. We terminated this process when the surface met the desired As/Ga ratio, VB shape, and E_F position. All thermal desorption were followed by a fast recovery of specimen temperature, typically ~250 °C in <1 min. A Cryogenics-CTI closed cycle refrigerator cooled the specimen and remained on at all stages of the experiment. The temperature of the specimen holder varied <20 K during each heating cycle, measured by a (7% Fe-Au)/Chromel thermocouple. The specimen temperature was monitored by the thermocouple and compared with the CLS temperature determination. We measured a 0.07-eV shift in the band-to-band transition during the cooling of the specimen. Such a

shift indicates a temperature of ~90 K, consistent with the thermocouple reading, and indicates a GaAs band gap of ~1.5 eV. We refer to ~90 K as LT (low temperature) in the text. Resistively heated tungsten coils evaporated Al and Au at background pressures less than 8×10^{-10} Torr. A quartz crystal microbalance monitored the rate of the deposition.

III. GaAs(100) VICINAL SURFACES

The oriented (100) surface is known to exhibit a rich variety of reconstructions depending on the surface composition.[17–19] A recent scanning-tunneling-microscopy (STM) study reveals the following surface structures in the order of increasing surface Ga concentration: $c(4\times4)$, 2×4, $c(2\times8)$, 2×6, 4×2 [which is usually seen as 4×6 in low-energy electron diffraction (LEED)], $c(8\times2)$, and evidence of 4×6 LEED order.[20] A calculation of the Ga-stabilized (100)-2×1 surface indicates Ga vacancies and surface nonmetallicity.[21] Calculations of the As-stabilized (100)-2×4 surface have predicted missing As dimers which promote the coexistence of many possible alignments of 2×4 cells.[22] SXPS investigations have demonstrated the existence of multiple surface-shifted components related to the As-rich surface reconstructions.[23,24] A phase diagram of surface structures versus As coverage as well as the ratio of Ga $3d$ to As $3d$ measured in SXPS has also been established.[17] Past SXPS studies reveal that small variations in surface stoichiometry, core-level line shape, [Ga]/[As] ratio, and valence-band shape actually correspond to different surface reconstruction phases.[17,23,24]

The vicinal GaAs(100) surfaces consist of domains of reconstructed (100) surfaces separated by steps.[25] The direction of the surface misorientation determines the nature of the bonding and consequently influences the topography of the step edge. A reflection-high-energy-electron-diffraction (RHEED) study indicates that the average terrace width is equivalent to single stepped staircases.[26] For instance, an 80-Å average separation is observed for 2° off GaAs(100) in the [111] direction.[26] Another RHEED study shows larger terrace width variation for misorientation toward $[111]_A$ than toward $[111]_B$ but smaller step-edge disorder for misorientation toward $[111]_A$ than toward $[111]_B$.[27] For an As-rich GaAs(100) surface with 2×4 reconstruction, a recent STM investigation reveals that the step edges are straight for dimers parallel to the step edge and jagged for dimers perpendicular to the step edge.[25] For vicinal GaAs(100) surfaces, configurations for the [110] step and for [111] steps with other than the 2×4 terrace reconstruction are not yet known.

Vicinal GaAs(100) surfaces are known to promote epitaxial growth and the direction of misorientation influences the film properties. For instance, surfaces misoriented in $[111]_A$ yield smoother morphology than $[111]_B$ for GaAs grown on vicinal Si (100) surfaces.[27] $Al_xGa_{1-x}As$ grown on GaAs(100) surfaces misoriented toward $[111]_A$ has not only improved morphology but also improved optical and electrical properties.[28]

We have constructed a ball-and-stick model for the unreconstructed, staircaselike GaAs(100) surface to show the vicinal steps. Displayed in Figs. 1(a), 1(b), and 1(c), respectively, are Ga-terminated GaAs(100) surfaces misoriented in the directions of [110], $[111]_A$, and $[111]_B$. The step height shown in Fig. 1 is $a_0/2$, where a_0 is the lattice constant of GaAs (5.656 Å). For 1°, 2°, and 4° angles of tilting from the (100) surface normal, ter-

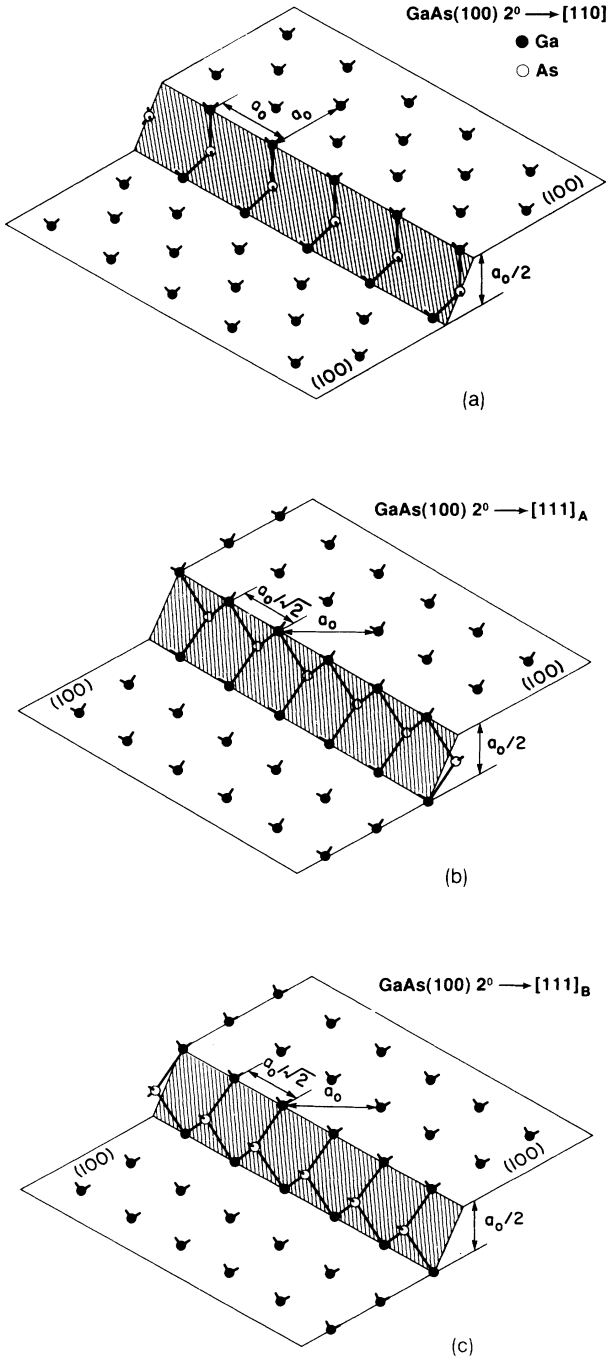

FIG. 1. Ball-and-stick model for unreconstructed, Ga-terminated, staircaselike vicinal GaAs(100) surfaces misoriented in the [110] (a), $[111]_A$ (b), and $[111]_B$ (c) directions. A or B here represent Ga or As atoms on the vicinal steps, respectively.

race separations are 162.0, 81.0, and 40.5 Å, respectively. The step densities are 6.17×10^5, 1.23×10^6, and 2.47×10^6 steps/cm, respectively. The steps on the (100)2°→[110] surface are parallel to the [100] direction with a separation of a_0 between dangling bonds along the step. Steps on the (100)2°→[111] surfaces are parallel to the [110] direction with dangling bonds at a separation of $a_0/\sqrt{2}$. As illustrated in Fig. 1, for the same angle of tilting, misorientation in the [111] direction produces a higher number of bonding sites per step than the [110] direction. Also illustrated by the model is the difference in the bonding nature between the step edges due to different misorientation. The [110] misorientation has As atoms in the plane of the step edge (shaded region) with dangling bonds at a 45° angle with respect to the step edge. The $[111]_A$ has As atoms below the plane of the step edge with Ga dangling bonds perpendicular to the step edge while the $[111]_B$ has As atoms above the plane of the step edge with As dangling bonds perpendicular to the edge.

We monitored the desorption of the As cap by examining the As/Ga ratio, E_F, and the VB spectrum. The desorption is judged complete when the As/Ga ratio reaches 0.9 in SXPS and when further desorption produces little or no changes in CLS spectra. The corresponding VB features were sharp and comparable to that obtained for the GaAs(110) cleaved surface.[29] The starting E_F were 0.2–0.3 eV from the conduction-band minimum and were obtained only after the full desorption procedure. The SXPS-determined and CLS-determined surfaces were consistent.

In comparison with the phase diagram of surface structure versus As/Ga ratios proposed by Bachrach,[17] the As/Ga ratio measured here indicates Ga-rich surfaces with reconstructions of $c(8\times2)$ and/or 4×6. The STM study shows that the $c(8\times2)$ reconstructed surface exhibits almost no surface As and the 4×6 reconstructed surface is obtained after further annealing at higher temperature.[18] Our recent LEED studies of decapped surfaces clearly show $c(8\times2)$ and/or diffuse 4×6 structures after final desorption.[30] SXPS line-shape analysis of clean surfaces indicates a single surface-shifted As component. For Ga, line-shape analysis suggests also a single surface-shifted feature. Since the configuration of step edges for $c(8\times2)$ and 4×6 terrace reconstruction are not yet known, in the following discussion we refer to the ball-and-stick diagram shown in Fig. 1 for densities of step-related bonding sites.

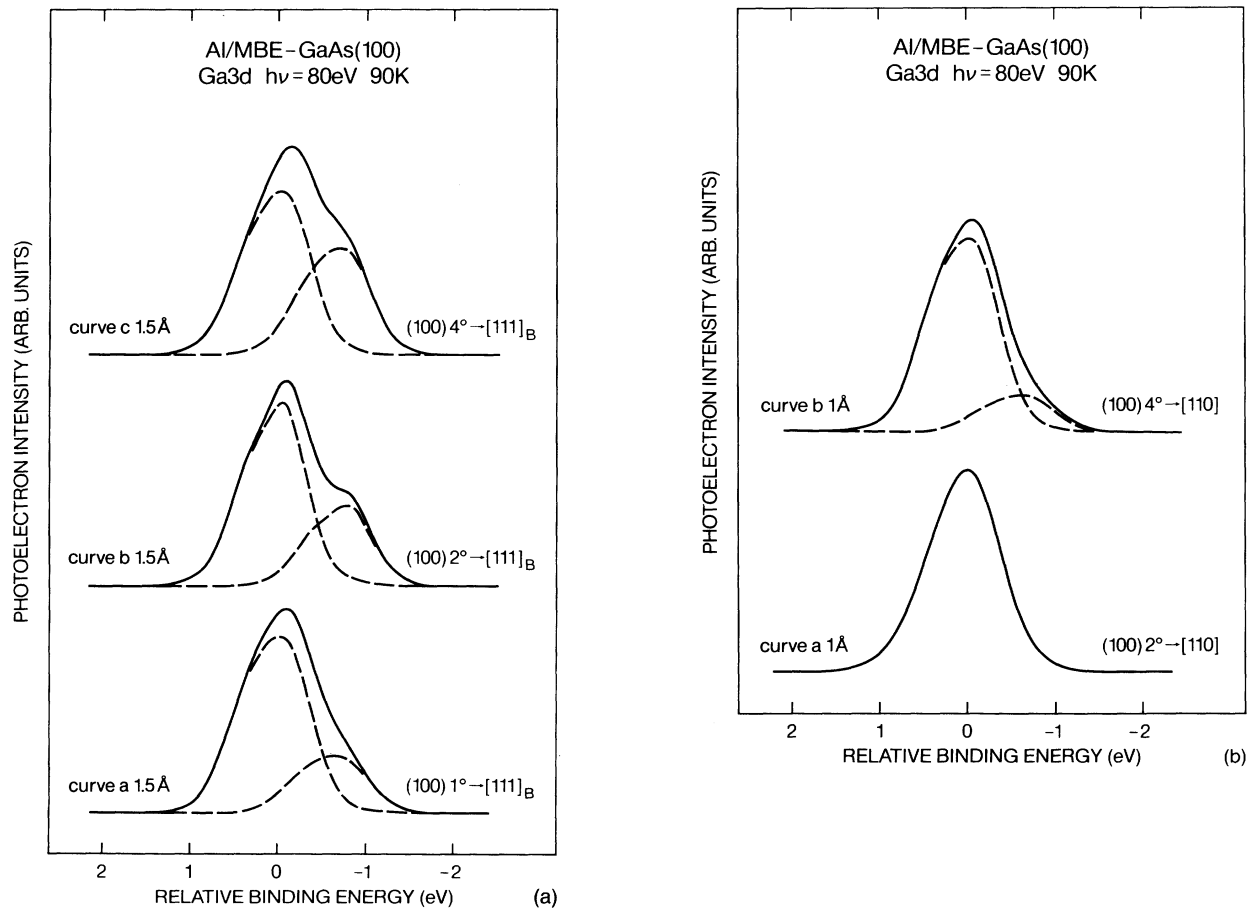

FIG. 2. Ga 3*d* core-level-spectra for (a) 1.5-Å Al on the GaAs(100)→$[111]_B$ surface and (b) 1-Å Al on the GaAs(100)→[110] surface. Dissociated Ga 3*d* peaks reveal an increasing extent of interface chemistry with increasing angle of misorientation.

IV. RESULTS

A. Orientation-dependent interface chemistry

1. The Al/GaAs(100) vicinal interface

For misoriented surfaces with a given misorientation direction, we observe an increase in the relative intensity of the dissociated Ga 3*d* component to the substrate Ga 3*d* component with increasing angle. In Fig. 2, the surface-sensitive (80-eV) Ga 3*d* core emissions are plotted at increasing degree of misorientation and normalized to the same peak height to emphasize the difference in line shapes. The zeros on the binding-energy axis indicate the position of the substrate Ga 3*d* component after subtracting band bending. For 1.5 Å of Al on GaAs(100)→$[111]_B$ [Fig. 2(a)], the ratio of the dissociated Ga to the substrate Ga increases from 0.34 to 0.45 to 0.66 with increasing tilting angle from 1° to 2° to 4°. Figure 2(b) indicates similar tilting angle-dependent interface chemistry for 1-Å Al deposited on the GaAs(100)→[110] surface. The ratio of dissociated Ga to substrate Ga increases from below our detection limit at 2° to 0.19 at 4°.

The Al/[vicinal GaAs(100)] interface chemistry also depends on the direction of misorientation. Figure 3 shows EDC's of the Ga 3*d* core spectra for 1.5-Å Al deposited on GaAs(100) surfaces 4° off axis toward [110], $[111]_A$, and $[111]_B$, respectively. The Ga 3*d* core spectra are again plotted with similar peak heights to show changes in line shape and have been compensated for band bending. Figure 3 reflects a changing ratio for the dissociated Ga to the substrate Ga upon varying substrate misorientation direction; values of 0.40, 0.55, and

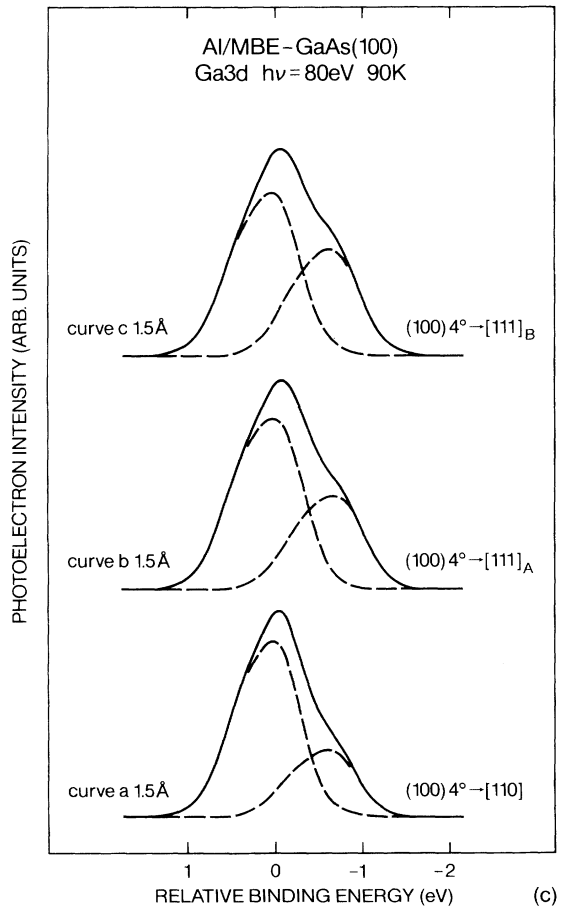

FIG. 3. Ga 3*d* core-level spectra for 1.5-Å Al deposited on the 4° misoriented GaAs(100) surfaces. Dissociated Ga 3*d* peaks reveal a variation of the extent of interface chemistry in accordance with the direction of misorientation, reflecting the role of the atomic bonding on the steps in the interface chemistry.

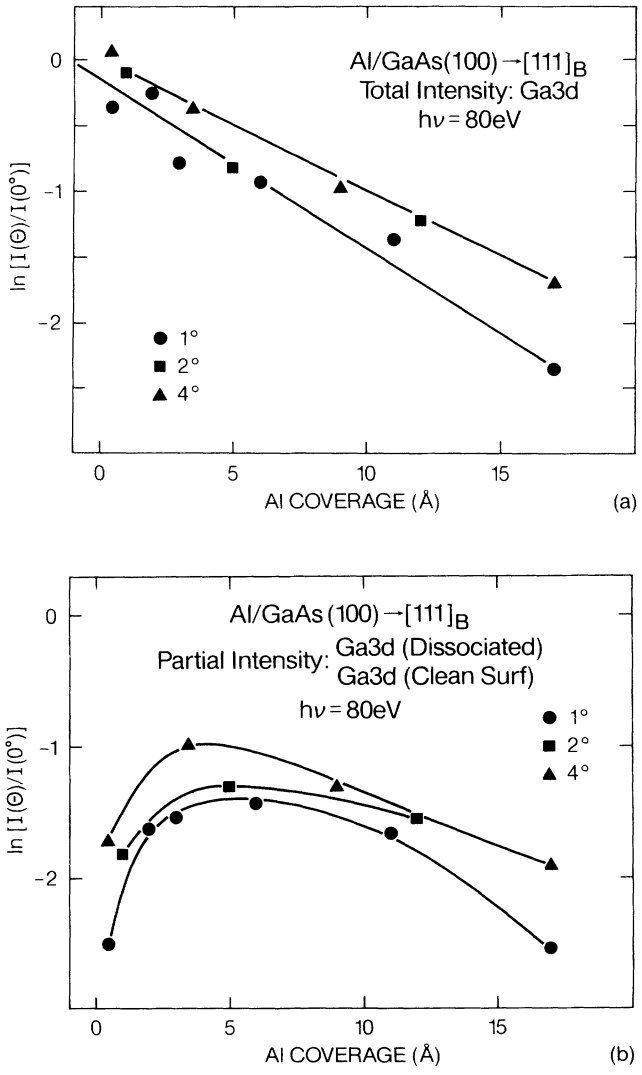

FIG. 4. Attenuation profiles of total Ga 3*d* emission intensities (a) and dissociated Ga 3*d* emission intensity (b) for Al/GaAs(100)→$[111]_B$ interfaces. Differences in the total Ga 3*d* emission decay rate (drawn for 10- and 6.5-Å attenuation lengths) among these vicinal interfaces reflect increasing Ga segregation. The distribution of the dissociated Ga atoms in the probing depth reveals the localized nature of the interface reaction.

0.66 are observed for [110], $[111]_A$, and $[111]_B$ directions of misorientation. Previously, we have reported similar orientation-dependent interface chemistry for 5-Å Al on various 2° misoriented GaAs(100) surfaces.[31,32]

Attenuation profiles for the Ga 3*d* core emission also exhibit an orientation dependence. Figure 4(a) displays profiles for total Ga 3*d* emissions ($h\nu=80$ eV) from Al/GaAs(100)→$[111]_B$ interfaces misaligned 1°, 2°, and 4°. The straight lines are provided as a guide to the eye to reflect attenuations for the Al/GaAs(100)→$[111]_B$ interfaces misoriented at a different degree. These Ga 3*d* emission intensities exhibit exponential decays. The decay rate, however, appears to decrease slightly upon increasing the misorientation angle. We obtained 10- and 6.5-Å attenuation length for the two lines shown. The spatial distributions of the dissociated Ga atoms are illustrated in Fig. 4(b). A comparison of the three Al/(100)→$[111]_B$ vicinal interfaces reveals a similar dependence of intensity versus Al coverage. The dissociated Ga increases and reaches a maximum concentration around 3–6-Å Al coverage. Above such a coverage, the exponential decay continues. The concentration of the dissociated Ga in the probing depth exhibits an overall increase with increasing misorientation.

The corresponding As 3*d* emissions exhibit little variation among vicinal surfaces. The As 3*d* line shape shows minimal changes upon Al deposition for all vicinal interfaces. The attenuation profiles, shown in Fig. 5, are indistinguishable within experimental uncertainty. These attenuation profiles appear to be best described by an exponential relationship. Such a relationship gives an attenuation length of 5 Å.

TABLE I. Percentage of Ga and As atoms with respect to the initial surface remaining in the sampling depth after 12-Å Au deposition. Comparison among these interfaces indicates that the extent of interdiffusion increases with increasing density of step-related structural sites.

Misorientation	I/I_0 (Ga 3*d*, 80 eV)	I/I_0 (As 3*d*, 100 eV)
(100)2°→[110]	0.19	0.13
(100)2°→$[111]_A$	0.29	0.25
(100)2°→$[111]_B$	0.26	0.22

2. *The Au/GaAs(100) vicinal interface*

Figure 6 shows nonexponential attenuations of Ga 3*d* and As 3*d* emissions for the Au/GaAs(100)2°→$[111]_B$ interface. The less surface-sensitive As 3*d* emission decays noticeably faster than the corresponding one for Ga, dropping to less than 6% of its initial value at 12 Å (not shown). Slightly higher Ga than As concentration in the sampling depth is observed for all Au interfaces. The attenuations of surface- and bulk-sensitive Ga 3*d* emissions are relatively comparable.

The misalignment of GaAs(100) surfaces can change the reduction rate of Ga 3*d* and As 3*d* core emissions for different vicinal interfaces. Table I shows, with respect to the clean surface, the percentage of the Ga and As atoms remaining in the sampling depth after 12-Å Au deposition on GaAs(100)2°→[110], 2°→$[111]_A$, and 2°→$[111]_B$ surfaces. Comparison indicates a higher extent of As and Ga concentrations in the probing depth

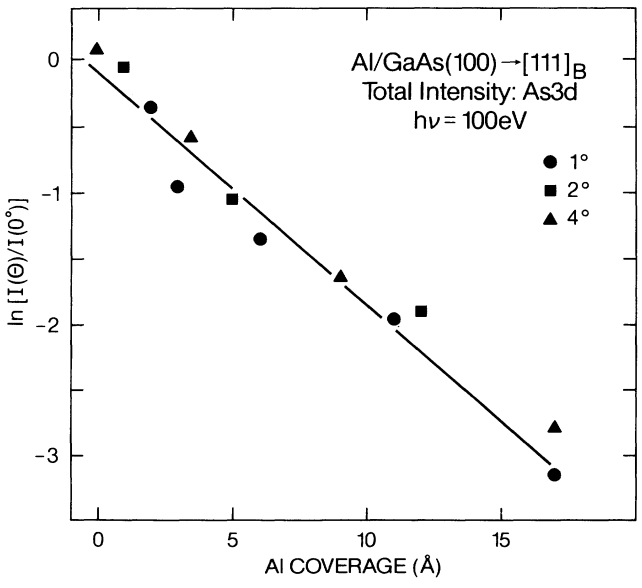

FIG. 5. Attenuation profiles of total As 3*d* emission intensities. The attenuation length (5 Å) indicates As trapping at the interface. The indistinguishable decay rates eliminates significant differences in morphology among Al/GaAs(100) vicinal interfaces.

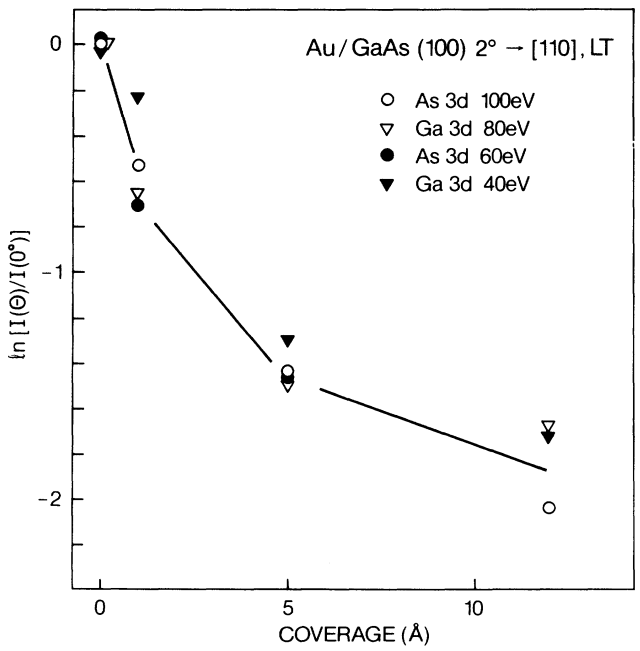

FIG. 6. Attenuation profiles of total Ga 3*d* and As 3*d* emission intensities for Au on the GaAs(100)2°→[110] surface. The nonexponential decay of the profiles shown here reflects the interdiffusive nature of the interface.

for Au/GaAS(100)→[111] interfaces relative to the Au/GaAs(100)→[110] interface. Between $[111]_A$ and $[111]_B$ interfaces, however, no significant difference is observed. The Ga and As emission reduction for the *A*-type interface might be slightly slower than for the *B*-type interface.

B. Orientation-dependent interface electronic properties

1. *Metallization of GaAs(100) vicinal surfaces*

Figure 7 shows the development of the VB and the VB edge as a function of Al coverage for the Al/GaAs(100)4°→$[111]_B$ interface to illustrate the establishment of an equilibrium E_F. The left EDC's illustrate the gradual evolution of a highly structured GaAs VB into a nearly featureless free-electron-like band upon increasing Al deposition. The right EDC's of VB edges show an initial near "flat-band" condition, which is common for all surfaces reported here. The topmost VB edge marks the E_F of the spectrometer. These VB edges indicate that by 9-Å coverage, E_F has reached its equilibrium value.

We have observed the above evolution for all Al and Au/GaAs(100) vicinal interfaces. For Al contacts, we have also observed the development of an asymmetric line shape in the Al 2*p* core-level emission accompanying the establishment of E_F. For Au/GaAs(100) vicinal interfaces, E_F converges to its equilibrium value by ~5 Å.

2. *Orientation-dependent Schottky-barrier height*

For given misorientation direction, the Schottky-barrier height at Al/[vicinal GaAs(100)] junctions appears to depend on the angle of misorientation. Figure 8 shows the position of E_F with respect to E_V as a function of Al coverages for GaAs(100)→$[111]_B$ surfaces misoriented 1° (circles), 2° (squares), and 4° (triangles). The E_F for clean surfaces are all located at 0.2–0.3 eV below the conduction-band minimum. For Al coverages <5 Å, $E_F - E_V$ increases with decreasing misorientation angle, approaching 0.92, 0.78, and 0.65 eV for metallic (≥10 Å) coverage.

The $E_F - E_V$ at Al/GaAs interfaces also depends on the misorientation direction. We have demonstrated pre-

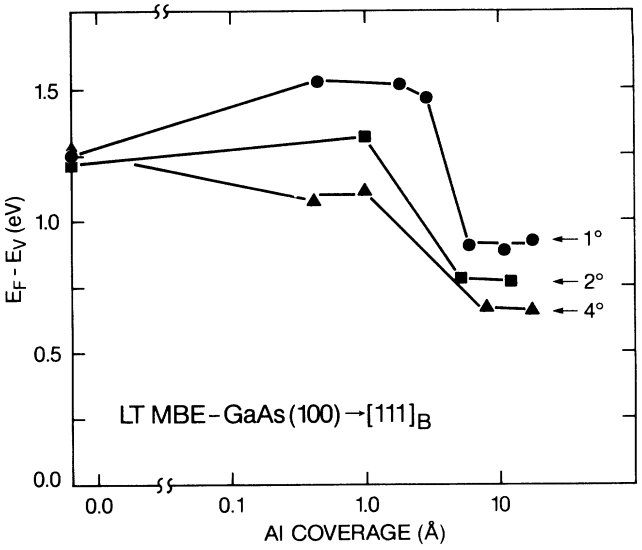

FIG. 8. E_F movement in the GaAs band gap as a function of Al deposition on GaAs(100)→$[111]_B$ surfaces. The final E_F reflects an increasing Schottky-barrier height with increasing angle of misorientation.

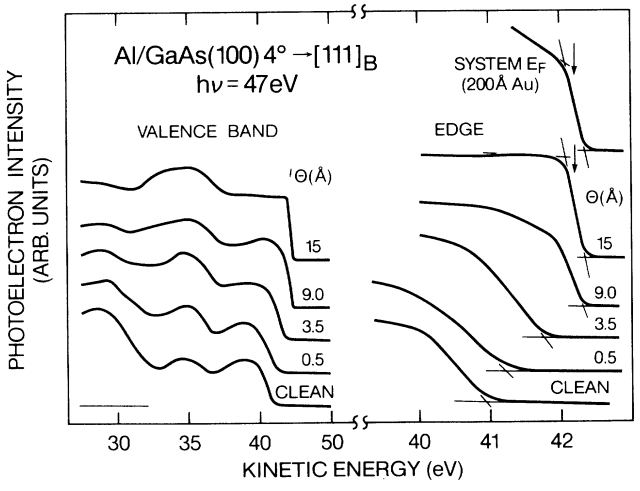

FIG. 7. Evolution of a highly structured GaAs VB into a nearly featureless free-electron band (left EDC's) and establishment of an equilibrium E_F (right EDC's). The VB evolution indicates complete surface metallization at the highest coverages.

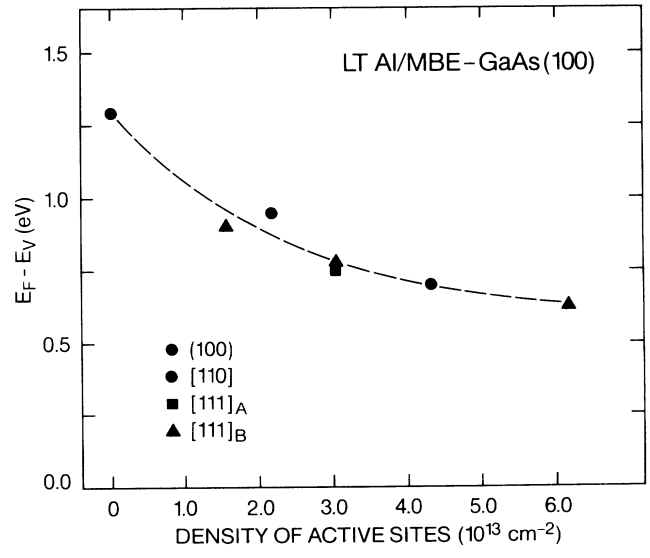

FIG. 9. Position of E_F with respect to the VB maximum vs density of step-related sites estimated by using the ball-and-stick model shown in Fig. 1. Inclusive of misorientation angles and directions, the barrier height at the Al/GaAs(100) vicinal interface increases with increasing density of active sites.

viously that as the misorientation direction for the 2° off-axis GaAs(100) surface changes from [110] to $[111]_A$ or $[111]_B$, the barrier height at the Al/GaAs vicinal interface varies from 0.55 to 0.76 eV.[31,32] For the aligned (100) surface, previous studies reported the barrier height could be as low as 0.2–0.3 eV for Al contacts.[11,12]

In Fig. 9 we show the correspondence between the measured Al/GaAs barrier height and the density of step-related bonding sites, inclusive of misorientation directions and angles. The defect densities are estimated from the ball-and-stick model shown in Fig. 1. Figure 9 shows that the barrier height increases monotonically as a function of active site density. A energy range of 0.65 eV is obtained between the aligned surface and the most "degraded" surface studied here (4°→$[111]_B$ (100) surface).

For Au/GaAs interfaces, our previous report has shown that the barrier height appears much less sensitive to the substrate misorientation.[31,32]

3. *Interface-specific electronic states*

The formation of electronic states in the band gap appears to be specific to the interface. We demonstrate this specificity by comparing the observed interface state formation at the misoriented Al and Au/GaAs interfaces to that at the corresponding aligned interfaces. In Figs. 10 and 11, respectively, we show CLS spectra for the Al aligned (a) versus misaligned (b) interfaces and the Au aligned (a) versus misaligned (b) interfaces. In each figure, spectra *a*, *b*, and *c* are for the clean surface, the metallized surface, and the difference curve between metallized and clean surfaces, respectively.

CLS spectra in Figs. 10(a), curve *a*, and 10(b), curve *a* exhibit intense band-to-band luminescence and weak deep-level emission within the band-gap characteristic for the clean MBE-grown GaAs.[13] Magnification of the below-band-gap region indicates spectral shape variations among surfaces. These variations appear to be minor when comparison is made between the aligned surfaces or between the misoriented surfaces, but more significant when comparing between the aligned and misoriented surfaces. Structureless and continuous emissions are typical for the clean (100) surface. For the 2°→[110] misaligned surface, the emission is weighted toward 0.9–0.95 eV.

Metal deposition introduces additional emissions in the below-band-gap region [Figs. 10(a), curve *b*, and 10(b), curve *b*]. Difference spectra—Figs. 10(a), curve *c*, and 10(b), curve *c*—between the metallized and the clean sur-

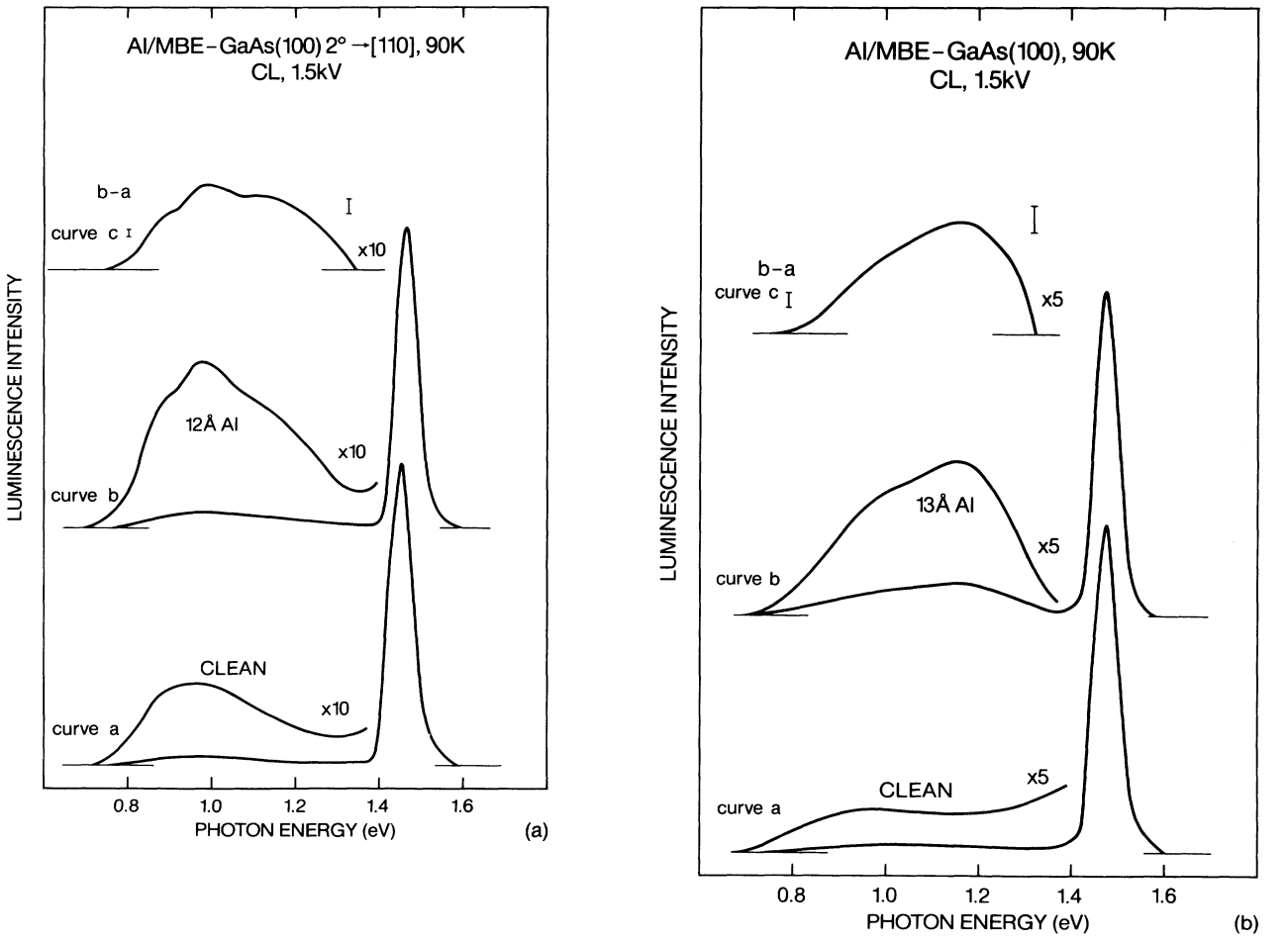

FIG. 10. CLS spectra from well-aligned (a) and misaligned (b) Al/GaAs(100) interfaces. Comparison indicates that Al deposition induces different electronic states: preferential emission at ~0.9–0.95 eV is observed for the misaligned interface.

faces emphasize the metal-induced emissions. The vertical bars here mark the uncertainty for these difference curves. Au induces relatively narrow optical emissions peaked around 1.2–1.25 eV for both aligned and 2°→[110] misaligned surfaces while Al introduces an overall emission enhancement over the entire below-band-gap energy range detectable for both surfaces.

The metal-induced states appear to be orientation dependent for the Al/GaAs(100) interface. For the oriented interface, the Al-induced emissions are weighted toward the 1.15-eV optical transition while for the misoriented interface, additional emission at 0.9–0.95 eV is observed.

V. DISCUSSION

A. Orientation-dependent interface chemistry

1. The Al/GaAs(100) vicinal interfaces

The dependence of the Al/GaAs interface chemistry on the misorientation angle indicates that the structural defects induced by the misorientation are chemically active. In fact, reactivity increases with the misorientation angle. Normalized to the initial clean surface, increasing the misorientation angle from 1° to 2° results in an ~5% increase of dissociated Ga in the probing depth. Upon further increasing the angle from 2° to 4°, one observes 9% more dissociated Ga in the sampling depth. This increase of the interface reaction versus the active site density demonstrates the effectiveness of these structural defects as nucleation sites for Al/GaAs interface reaction.

The dependence of the Al/GaAs interface reaction on the direction of misorientation reveals how interface chemical reactivity depends on the bonding sites available. We observe that Al is more reactive with *B*-type steps than *A*-type steps (Fig. 3).[26] Crystallographic orientation-dependent preferential chemical etching and oxidation indicates that As-terminated surfaces are more reactive than Ga-terminated surfaces.[33,34] The higher reactivity of *B*-type steps compared to *A*-type steps is likely to be due to As atoms being more available to bond Al in the former. We also observe that steps with Ga atoms in the $[111]_A$ direction are more reactive compared to steps in the [110] direction, although the ball-and-stick model (Fig. 1) shows that the [110] steps consist of As atoms. Three factors may contribute to this difference: (1) for the same degree of misorientation, the $[111]_A$ misoriented surface has more nucleation sites than the [110] misoriented surface, (2) for $[111]_A$, As atoms are still exposed although in the second layer and without a dangling bond, which may also have an effect

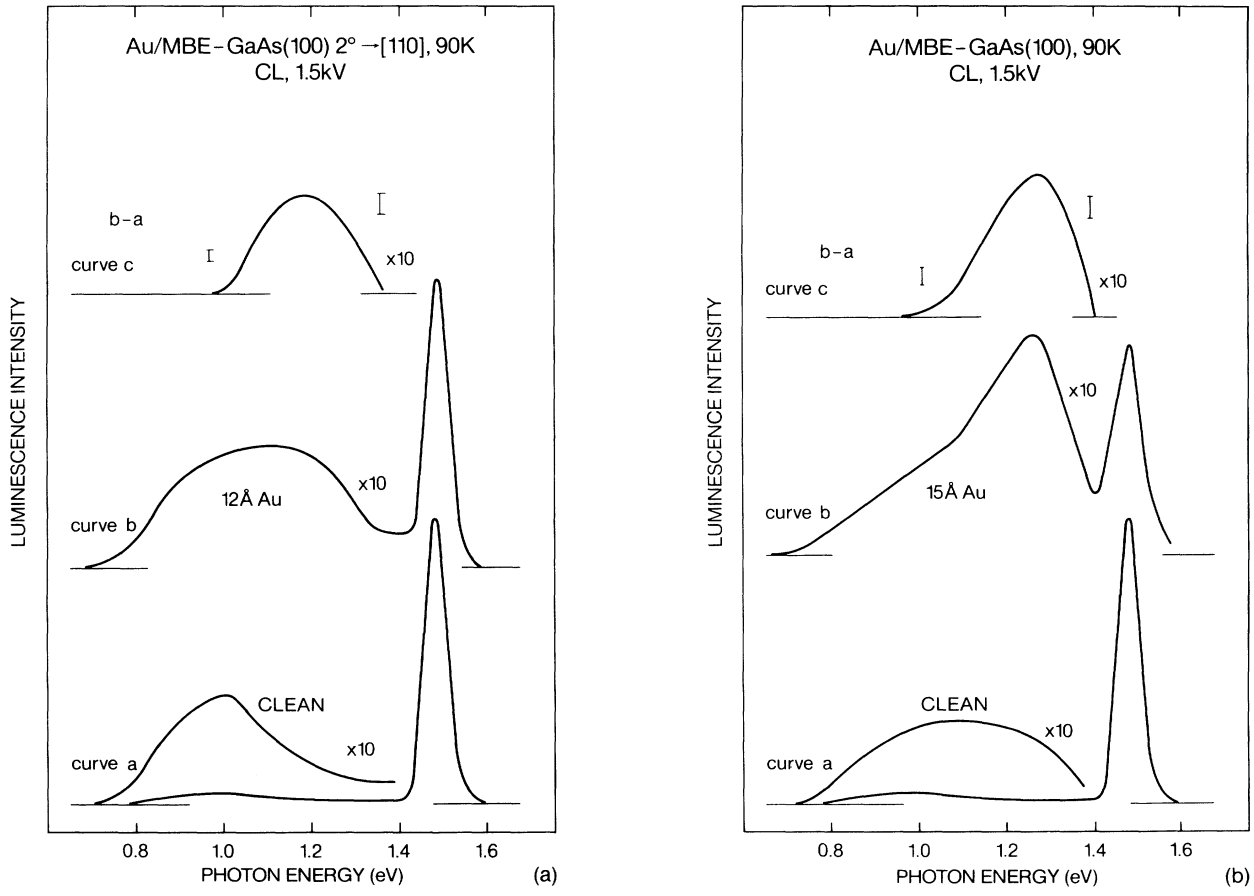

FIG. 11. CLS spectra from well-aligned (a) and misaligned (b) Au/GaAs(100) interfaces. Au deposition induces similar electronic states in the band gap for the two interfaces.

on the interface chemistry, and (3) the configuration of the $[111]_A$ step edge can be significantly different from that of the [110] step edge, resulting in variation of active site densities as well as the atomic structure of the edge (the relative position of the As atoms to the Ga atoms on the edges). STM results have recently shown that the step-edge configurations are indeed quite different for A and B steps on GaAs(100)-2×4 surfaces.[25]

With attenuation profiles, one can probe interface morphology and the overlayer growth. Epitaxial growth would give rise to an exponential attenuation as a function of layer thickness while clustering or interdiffusion would give a nonexponential dependence. The exponential attenuation of Ga and As 3d core emissions (Figs. 4 and 5) indicates that the Al growth is nearly layer by layer for different vicinal surfaces. A slight dependence of the attenuation profile on the misorientation is observed for the Ga 3d core emission [Fig. 4(a)] but not for the As (Fig. 5). Assuming similar uncertainty in the estimated Ga and As 3d emission intensity, the observed difference in the Ga 3d core emission attenuation length due to changing misorientation angle (Fig. 4) implies Ga segregation. The extent of this segregation depends on the misorientation angle. Epitaxial growth of an Al overlayer on GaAs(100) has been observed before. For instance, Al grows more homogeneously on GaAs(110) at 60 K due to the reduction in the mobility of Al atoms.[35] Growth of Al on GaAs(100) surfaces results in Al epitaxy with crystallinity dependent on the GaAs(100) surface reconstruction, the stoichiometry, the disorder, the growth temperature, and the growth rate.[36–40]

The spatial variation in the number of dissociated Ga atoms with depth [Fig. 4(b)] indicates a localized interface reaction, mostly within a 3–6-Å range of the interface. The relatively small electron escape length (5 Å) derived from the As 3d attenuation (which is less than the Ga 3d attenuation length) also reflects a localized interface region and As trapping at the interface. The 3–6-Å interface width implies that only a few layers of the interface are disrupted.

The Al/GaAs interface reaction has been characterized in the past as a replacement of Ga with Al to form AlAs and solid solution of Ga in the overlayer.[41] Formation of $Al_xGa_{1-x}As$ has been observed more recently after annealing at elevated temperatures.[41–43] For MBE-GaAs(100) surfaces, previous studies[36,40] have reported a partial replacement reaction for the Ga-terminated 4×6 surface at room temperature. Here, the absence of line-shape changes in the As 3d core rules out the formation of multiple cation-As compounds. The dissolution of Ga atoms from GaAs is mostly due to the formation of AlAs at the interface.

By comparison, Al on melt-grown GaAs(110) cleaved surfaces and on As capped/decapped MBE (100) surfaces differ in the following ways: (1) The Al/GaAs(110) interface reaction appears to be temperature independent,[35] while the Al/GaAs(100) interface reaction is reduced at lower growth temperature.[11,12] (2) At room temperature, Al clusters on the GaAs(110) surface, but can grow epitaxially on the (100) surface.[44] Perhaps the epitaxial Al/GaAs(100) relation inhibits chemical reaction to the same extent as observed for Al/GaAs(110), where no such epitaxial relation exists.

2. *The Au/GaAs vicinal interfaces*

Au deposition on GaAs(100) vicinal surfaces induces significant interdiffusion. The attenuation of both Ga 3d and As 3d core emissions shows nonexponential growth. The comparable decay rates between surface- and bulk-sensitive Ga 3d emissions underline the diffusive rather than island-formation nature of the interface. Clustered growth would have resulted in a nonexponential attenuation for which surface-sensitive emission decays faster than that of the bulk-sensitive emission.

For Au/GaAs(100) vicinal contacts, the step-related structural sites also play an important role in observed misorientation-dependent interdiffusion. The GaAs(100)→[111] surface has a higher density of step-related defect sites than the GaAs(100)→[110] surface, consequently the interdiffusion appears more extensive for the former than the latter (Table I).

However, the atomic bonding on the steps does not significantly affect the interface diffusion process between the A- and B-stepped surfaces. This apparent insensitivity may be attributed to the diffusive rather than the reactive nature of the interface. Bauer has reported that Au tends to agglomerate at pitted areas on etched GaAs(100) surfaces.[45] The A and B steps are equivalent in terms of sites for agglomeration and, consequently, showed here comparable diffusion processes. The overall reactivity of a Au/GaAs(100) vicinal interface thus depends on the number of defect sites available.

Past studies have shown Au/GaAs interface intermixing. The extent of the interdiffusion and the interface morphology, however, varies from surface to surface according to the growth condition. For instance, Au grown on a MBE-GaAs(100) surface at temperatures higher than 300 °C shows both interdiffusion and clustering.[46] Annealing of a room-temperature-grown Au/(MBE-GaAs) interface at 300 °C increases the surface content of Ga.[46] Subsurface As layer formation at Au/[MBE-GaAs(100)] interfaces has been observed.[47] Vermaak, Snyman, and Auret reported epitaxially grown Au on melt-grown, etched GaAs(100) surfaces and found that the epitaxial growth could be destroyed by carbon contamination.[48] These results reflect an interface-specific chemical activity. The orientation-dependent interface interdiffusion presented here is another demonstration for the importance of local atomic interface structure upon interface chemistry.

B. Orientation-dependent electronic properties

1. *Surface photovoltage (SPV)*

Recent studies have demonstrated that the magnitude of SPV during synchrotron radiation photoemission experiments can influence the determination of Schottky-barrier heights at metal-semiconductor interfaces, especially for low doped semiconductors at low temperature.[49] The SPV, however, can be eliminated by using highly doped semiconductors, semiconductors at elevated

temperatures, or semiconductors with conducting (metallized) surfaces.[49] The elimination of SPV through surface metallization depends sensitively on the conducting pathway. The conductance of the specimen surface, its sides, and the position of contacts to the surface are relevant. For instance, isolated metallic islands, preferentially grown at room temperature, have little effect on diminishing the photovoltaic charging.[49,50] More efficient electron conduction in homogeneous metallic films grown at low temperature compensates the reduced thermionic carrier recombination at these low temperatures.[51] Thus, metallic interfaces formed at low temperature appear to be more efficient in the elimination of SPV.[51]

Several methods have been proposed[51–55] to measure the magnitude of SPV: determining the dependence of E_F on the substrate temperature,[52,53,55] determining the difference between the E_F of the interface and that of the system,[50] and surface photovoltage spectroscopy.[54] The measured SPV can be used to correct the band bending and thus to obtain the actual Schottky-barrier height at metal-semiconductor interfaces.[51,54]

We observe no measurable SPV within our experimental uncertainty (<0.1 eV) at the thickest metal coverage. We have established that the interface E_F [for all metal/GaAs(100) interface systems] matches that of the spectrometer. Following the work of Alonso, Cimino, and Horn,[51] alignment of the Fermi cutoff for the metallized surface with the E_F of the system is indicative of negligible SPV.

2. *Orientation-dependent Schottky-barrier height and interface states*

The dependence of the Al/GaAs(100) barrier height on the misorientation angle implies that the misorientation-induced step sites are electrically active. We can also associate the larger barrier height at the Al/GaAs (100)→[111] interface over that at the Al/GaAs(100)→[110] interface with the higher active site density at the [111] misoriented surface.[31,32] Our observation that the E_F moves from $E_V+1.3$ eV (near the Schottky limit) to $E_V+0.65$ eV (Fig. 9) as a function of step-related active-site density indicates stabilization of the E_F at interface states located at $\leq E_V+0.65$ eV. Such a convergence implies a creation of electronic gap states due to substrate misorientation and reflects a correlation between the Al/GaAs interface electronic states and the surface structural sites.

CLS results show that misorientation introduces electronic states associated with an ~ 0.9-eV optical transition at the Al/GaAs(100) interface (Fig. 10). Evidence of the misorientation-induced states also appears in clean surface CLS spectra [Figs. 10(a), curve *a*, and 11(a), curve *a*]; however, their effect on band bending cannot be assessed by SXPS experiments due to the presence of the SPV on unmetallized surfaces.[52] At the Al/GaAs interface, the formation of these electronic gap states may be the cause for the E_F to move from the ideal Schottky position. The 0.9-eV optical transition corresponds to a gap state at $E_V+0.6$ eV, consistent with the convergence indicated by the E_F-E_V versus the density of active-site relationship (Fig. 9).

The Au/GaAs vicinal interfaces exhibit little variation (<0.15 eV) with respect to the surface misorientation, in contrast to the Al case (0.65-eV variation). Our results suggest that misorientation dependence of the barrier height is specific to the interface. Indeed, the gap states which affect the Schottky-barrier heights are different between the Al and Au/GaAs interfaces. CLS [Figs. 10(a), curve *c*, and 11(a), curve *c*] demonstrates that in contrast to Al deposition, Au deposition on misoriented surfaces apparently does not introduce additional states in the band gap.

Compared to MBE-GaAs(100) aligned surfaces, the MBE-grown vicinal surfaces differ in surface perfection. A review of past measurements in the literature further emphasizes the role of the local interface structure in the Schottky-barrier formation. Both Al/GaAs and Au/GaAs barrier heights vary according to physical parameters involved in forming the interface. This variation is particularly evident for the (100) interfaces where the initial surface possesses a variety of reconstruction. For Al interfaces, Al barrier heights between 0.62 and 0.83 eV have been reported for various GaAs(100) surface reconstructions.[37,56–61] In fact, different Al barrier heights have been reported by different research groups for the same surface reconstruction. For an *n* type GaAs(100)-*c*(2×8) surface, Zhang *et al.*[43] measured a barrier height of 0.62 eV and Al/GaAs interfaces, while Svensson, Landgren, and Andersson,[57] Cho and Dernier,[56] and Wang[59] reported 0.76 eV, both using the current-voltage technique. Other than the unprecedentedly low Al barrier height observed in SXPS for Al on the low-temperature, MBE-grown, Ga-rich GaAs(100) prepared by the As-capping/decapping procedure described here, Barret and Missous[60] measured an Al barrier height as low as 0.55 eV using the current-voltage technique, however with a poor ideality factor. Sun *et al.*[61] showed that the Al barrier height depends systematically on the sample history. Okamoto[62] also reported a barrier height dependence on the Al deposition condition. Recently, Costa *et al.*[63] have shown that by varying the deposition condition of a Si interlayer, the Al barrier height changes significantly between 0.3 and 1.04 eV. For Au/GaAs interfaces, similarly, barrier heights between 0.9 eV (Refs. 64 and 65) and 1.1–1.2 eV (Ref. 66) have been reported. Examples of band bending according to the interface-preparation–surface morphology can be extended to many other systems. For instance, barrier heights of 0.83 and 0.97 eV are observed for Ag on GaAs(100)*c*(2×8) and (100)4×6, respectively;[67] $NiSi_2$ on Si results in different barrier heights depending on the epitaxial relationship;[68] and the E_F pins at energies associated with dislocations on the surface.[69] Recently, Palmstrøm *et al.* have demonstrated a large variation in barrier height for epitaxy ErAs on GaAs depending on the GaAs surface orientation.[70] Thus, E_F apparently does not "pin" at a fixed energy position in the gap and the differences in barrier heights among various measurements can be attributed to the interface-specific electronic properties.[71–73]

3. *Correlation of interface states versus step-induced active sites*

The aforementioned relationship between barrier heights, interface states, and active site densities can be established by using a self-consistent electrostatic analysis proposed by Mailhiot and Duke.[74] The barrier height is calculated versus metal work function for a given semiconductor. The calculation includes shifts in barrier height due to the formation of an interface dipole. The shift in the interface dipole caused by subsurface traps can be matched to experimental measurements, and in this way one can extract the density and energy of the charged interface states. Specifically, by fixing the energies and the nature (acceptor or donor) of the charge states, we can calculate the deviation in barrier heights from the ideal Schottky limit in terms of the density of these charge states at the metal-semiconductor interface.

We have selected the energy of the charge states based on our CLS results. CLS measures a transition associated with steps at 0.9 eV, and a transition intrinsic to the surface at ~ 1.25 eV. We have chosen an acceptor state at $E_V + 0.6$ eV, corresponding to the 0.9-eV transition observed. For a large enough acceptor state density, E_F is expected to pin at the acceptor level. In our previous analysis of misoriented interfaces, we used a 0.8-eV acceptor state, consistent with several metals on oriented GaAs(100).[12] However, for the misoriented surfaces, a variable density of the 0.6-eV acceptor state appears more appropriate. The ~ 1.25 eV transition corresponds to an acceptor state intrinsic to the semiconductor at $\sim E_V + 0.2$ eV. A fixed density of $5 \times 10^{12}/\text{cm}^2$ best fits the obtained Au barrier heights for both oriented and misoriented surfaces. Aside from the assumption that these charge states lie 10 Å below the semiconductor surface away from the interface, no other adjustable parameters are involved in the analysis. (Numerical results would be somewhat different if the position of defect would change. 10 Å here is a representative number.)

We display in Fig. 12 a family of curves presenting the results of the analysis for the Al/GaAs(100) vicinal interfaces for various interface state densities. Figure 12 shows that the Al/GaAs barrier height increases with the density of 0.6-eV acceptor states, while the Au barrier heights are insensitive to the 0.6-eV acceptor state density. This overlayer dependence occurs because the 0.2-eV acceptor states mostly affect the barrier properties for the the high work-function metals while the midgap acceptor influences the behavior of Schottky barrier for lower work-function metals.[12]

From this family of plots, we can determine the density of the 0.6-eV acceptor state that gives rise to the measured barrier height at Al/GaAs(100) vicinal interfaces. Figure 13 plots the density of the 0.6-eV acceptor state determined from experiments versus the density of step-related active sites determined by the geometry of the unreconstructed steps. The straight line drawn is determined by linear regression. The slope of this straight line is 0.61. The error bars follow from a rigorous convolution of the uncertainty in density due to the 0.05-eV CLS resolution in measurement of the acceptor-state energy and a 0.05-eV precision in the core-level shift measurement. The large upper error bar at the highest active site density is due to the asymptotic behavior near the E_F stabilization energy, where small deviations in the E_F position causes large variations in the density of interface states.

The slope of 0.61 in Fig. 13 suggests that Al metallization of each chemically active site at a step produces the equivalent of $\sim \frac{2}{3}$ acceptor charges. A proportionality greater than unity would imply that the misorientation-induced charge site at the interface alone could not produce the measure barrier height or that the charge site resides farther than 10 Å below the surface. Extrapolation of the linear dependence gives a density of 1.1×10^{13} cm^{-2} for the 0.6-eV state at the oriented GaAs(100) sur-

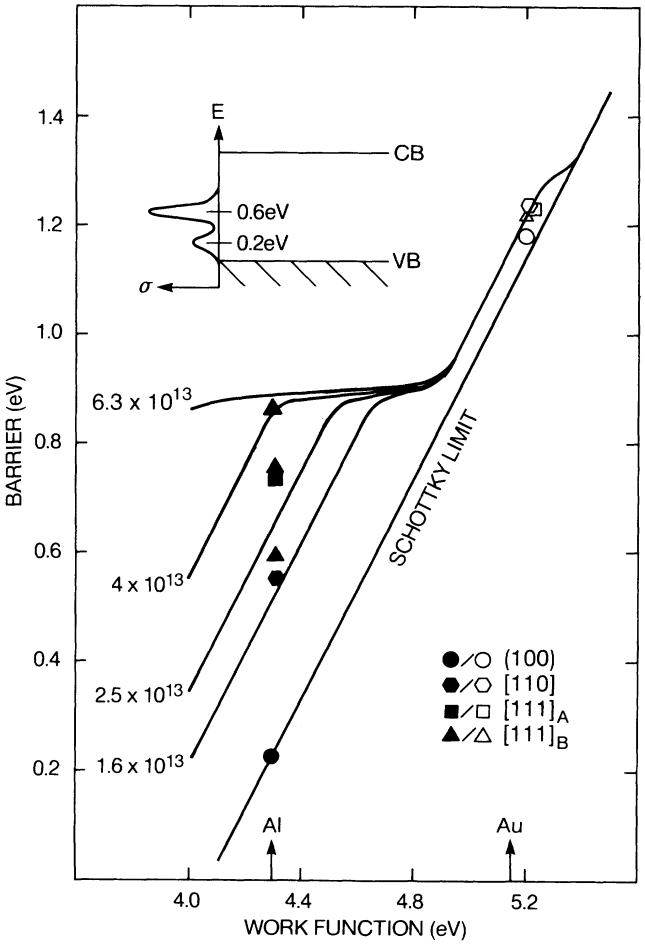

FIG. 12. Self-consistent electrostatic analysis of barrier heights at Al and Au/GaAs(100) vicinal interfaces. The family of plots represents a fixed acceptor state density of 5×10^{12} cm^{-2} at $E_V + 0.2$ eV and varied acceptor state densities at $E_V + 0.6$ eV (see inset). Increasing Al barrier heights correspond to increasing midgap state densities, underlining a correlation between the density of midgap states vs the density of step-related active sites.

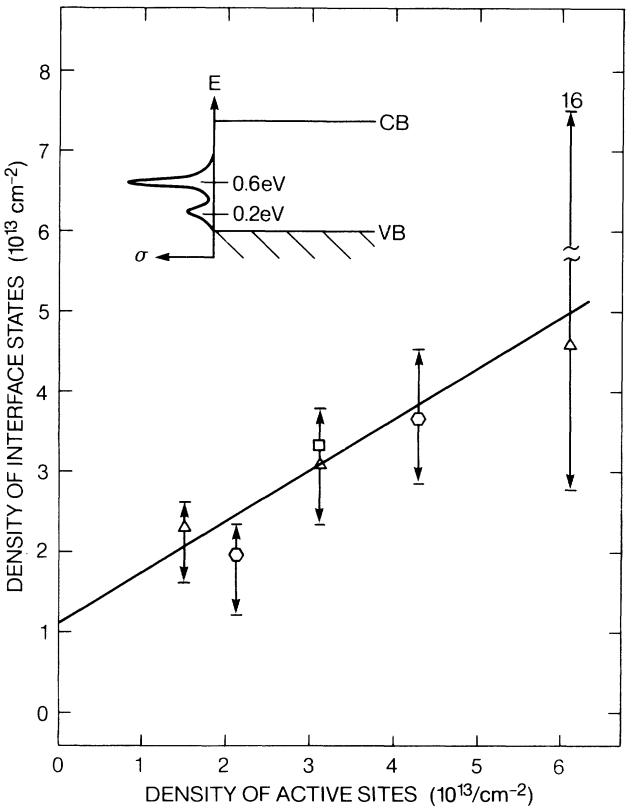

FIG. 13. Relationship between the density of the 0.6-eV acceptor state (extracted from Fig. 12) and the density of step-related sites (extracted from Fig. 1). The linear correspondence emphasizes the role of misorientation-induced active sites in the formation of interface states. The slope suggests that each active site creates $\sim\frac{2}{3}$ acceptor charge and the extrapolation indicates a low density (1.1×10^{13} cm^{-2}) of the 0.6-eV state for the aligned Al/GaAs(100) interface.

face, confirming previous CLS results showing a low interface state density for metals on the well aligned surfaces.[13,15,75] Although this correlation fixes the depth of the interface states and estimates the active site densities from unreconstructed, staircaselike steps, the nearly one-to-one correspondence demonstrates the role of misorientation-induced bonding sites in the formation of interface states. Such a relationship may be useful in establishing a tradeoff between epitaxial growth efficiency and electronic perturbation.

Finally, in comparison to the various models for Schottky-barrier formation, our results do not support models that predict the E_F pinning and its insensitivity to the interface conditions.[6–9] Our observations indicate instead that the details of chemical activity at the intimate interface influence the contact electronic properties and their relation to the ideal Schottky behavior.

VI. CONCLUSION

We have demonstrated an orientation-dependent interface chemistry and electronic barrier formation for Al on GaAs(100) misoriented surfaces. We have provided evidence for the importance of local interface structure on the macroscopic contact electronic properties. By extracting deep-level densities from the E_F stabilization energies measured by SXPS and the deep-level energies measured by CLS, we have established a relationship between the interface states near midgap and the chemically active sites believed due to misorientation. Overall these results show that intentionally misoriented GaAs substrates commonly used to facilitate epitaxial growth can have major effects on the interface electronic properties.

ACKNOWLEDGMENTS

This work was supported in part by the Office of Naval Research under Contract No. N00014-80-C-0778. The Synchrotron Radiation Center at the University of Wisconsin, Madison, is supported by the National Science Foundation.

[1]See, for example. L. J. Brillson, Surf. Sci. Rep. **2**, 123 (1982); Comments Condens. Matter Phys. **14**, 311 (1989).

[2]I. Lindau and T. Kendelewicz, CRC Rev. Solid State Mater. Sci. **13**, 27 (1986).

[3]J. H. Weaver, in *Electronic Materials: A New Era of Materials Science,* edited by J. R. Chelikowsky and A. Franciosi (Springer-Verlag, Berlin, 1991), Chap. 8, p. 135.

[4]E. H. Rhoderick and R. H. Williams, *Metal-Semiconductor Contacts,* 2nd ed. (Clarendon, Oxford, 1988).

[5]W. Schottky, Naturwissenschaften **26**, 843 (1938); Z. Phys. **113**, 367 (1939).

[6]V. Heine, Phys Rev. **138**, A 1689 (1965).

[7]J. Tersoff, Phys. Rev. Lett. **52**, 465 (1984).

[8]W. E. Spicer, I. Lindau, P. Skeath, and C. Y. Su, J. Vac. Sci. Technol. **17**, 1019 (1980); W. E. Spicer, T. Kendelewicz, N. Newman, R. Cao, and E. R. Weber, J. Vac. Sci. Technol. B **6**, 1245 (1988).

[9]R. H. Williams, R. R. Varma, and V. Montgomery, J. Vac. Sci. Technol. **16**, 1418 (1979).

[10]J. L. Freeouf and J. M. Woodall, Appl. Phys. Lett. **39**, 727 (1981); J. M. Woodall and J. L. Freeouf, J. Vac. Sci. Technol. **19**, 794 (1981).

[11]R. E. Viturro, J. L. Shaw, C. Mailhiot, L. J. Brillson, N. Tache, J. McKinley, G. Margaritondo, J. M. Woodall, P. D. Kirchner, G. D. Pettit, and S. L. Wright, Appl. Phys. Lett. **52**, 2052 (1988).

[12]R. E. Viturro, S. Chang, J. L. Shaw, C. Mailhiot, L. J. Brillson, A. Terrasi, Y. Hwo, G. Margaritondo, P. D. Kirchner, and J. M. Woodall, J. Vac. Sci. Technol. B **7**, 1007 (1989).

[13]R. E. Viturro, J. L. Shaw, L. J. Brillson, J. M. Woodall, P. D. Kirchner, G. D Pettit, and S. L. Wright, J. Vac. Sci. Technol. B **6**, 1397 (1988).

[14]J. L. Shaw, L. J. Brillson, S. Sivananthan, and J. P. Faurie, Appl. Phys. Lett. **56**, 1266 (1990).

[15]R. E. Viturro, M. L. Slade, and L. J. Brillson, J. Vac. Sci.

Technol. A **5**, 1516 (1987).
[16]M. C. Schabel, I. M. Vitomirov, G. D. Waddill, and J. H. Weaver, J. Electron Spectrosc. Relat. Phenom. **56**, 211 (1991).
[17]R. Z. Bachrach, R. S. Bauer, P. Chiaradia, and G. V. Hansson, J. Vac. Sci. Technol. **19**, 335 (1981).
[18]A. Y. Cho, J. Appl. Phys. **42**, 2074 (1971).
[19]P. Drathen, W. Ranke, and K. Jacobi, Surf. Sci. **77**, L162 (1978).
[20]D. K. Biegelsen, R. D. Bringans, J. E. Northrup, and L.-E. Swartz, Phys. Rev. B **41**, 5701 (1990).
[21]D. J. Chadi, J. Vac. Sci. Technol. A **5**, 834 (1987).
[22]P. K. Larsen and D. J. Chadi, Phys. Rev. B **37**, 8282 (1988).
[23]J. E. van der Veen, P. K. Larsen, J. H. Neave, and B. A. Joyce, Solid State Commun. **49**, 659 (1984).
[24]R. Ludeke, T.-C. Chiang, and D. E. Eastman, Physica **117B&118B**, 819 (1983).
[25]M. D. Pashley, K. W. Haberern, and J. M. Gaines, Appl. Phys. Lett. **58**, 406 (1991).
[26]S. A. Chalmers, A. C. Gossard, P. M. Petroff, J. M. Gaines, and H. Kroemer, J. Vac. Sci. Technol. B **7**, 1357 (1989).
[27]P. R. Pukite, G. S. Petrich, S. Batra, and P. I. Cohen, J. Cryst. Growth **95**, 269 (1989).
[28]L. Däweritz and R. Hey, Surf. Sci. **236**, 15 (1990).
[29]R. E. Viturro, C. Mailhiot, J. L. Shaw, L. J. Brillson, D. LaGraffe, G. Margaritondo, G. D. Pettit, and J. M. Woodall, J. Vac. Sci. Technol. A **7**, 855 (1989).
[30]I. M. Vitomirov, R. E. Viturro, S. Chang, and L. J. Brillson (unpublished).
[31]S. Chang, L. J. Brillson, Y. J. Kime, D. S. Rioux, P. D. Kirchner, G. D. Pettit, and J. M. Woodall, Phys. Rev. Lett. **64**, 2551 (1990).
[32]S. Chang, L. J. Brillson, D. F. Rioux, Y. J. Kime, D. P. Kirchner, G. D. Pettit, and J. M. Woodall, J. Vac. Sci. Technol. B **8**, 1008 (1990).
[33]H. C. Gatos, P. L. Moody, and M. C. Lavine, J. Appl. Phys. **31**, 212 (1960).
[34]*Properties of Gallium Arsenide,* 2nd ed. (INSPEC, The Institute of Electrical Engineering, New York, 1986).
[35]S. G. Anderson, C. M. Aldao, G. D. Waddill, I. M. Vitomirov, S. J. Severtson, and J. H. Weaver, Phys. Rev. B **40**, 8305 (1989).
[36]R. Ludeke and G. Landgren, J. Vac. Sci. Technol. **19**, 667 (1981).
[37]J. Massies and N. T. Linh, Surf. Sci. **114**, 147 (1982).
[38]S. K. Donner, K. P. Caffey, and N. Winograd, J. Vac. Sci. Technol. B **7**, 742 (1989).
[39]S. K. Donner, J. L. Herman, R. Blumenthal, R. Trehau, E. Furman, and N. Winograd, Appl. Phys. Lett. **55**, 1753 (1990).
[40]G. Landgren, S. P. Svensson, and T. G. Andersson, Surf. Sci. **122**, 55 (1982).
[41]A. Kahn, L. J. Brillson, and C. B. Duke, Phys. Rev. Lett. **42**, 397 (1979).
[42]S. A. Chambers, Phys. Rev. B **39**, 12 664 (1989).
[43]Z. Zhang, Z. Chen, Y. Xing, D. Sun, and G. Shea, Chin. Phys. **6**, 1057 (1986).
[44]N. G. Stoffel, M. Kelly, and G. Margaritondo, Phys. Rev. B **27**, 6561 (1983).
[45]C. L. Bauer, Surf. Sci. **168**, 395 (1986).
[46]T. G. Andersson, J. Kanski, G. Le Lay, and S. P. Svensson, Surf. Sci. **168**, 3301 (1986).
[47]J. Kanski, S. P. Svensson, T. G. Andersson, and G. Le Lay, Solid State Commun. **54**, 339 (1985).
[48]J. S. Vermacek, L. W. Snyman, and F. D. Auret, J. Cryst. Growth **42**, 132 (1977).
[49]M. H. Hecht, Phys. Rev. B **41**, 7819 (1990).
[50]G. D. Waddill, T. Komeda, Y.-N. Yang, and J. H. Weaver, Phys. Rev. B **41**, 10 283 (1990).
[51]M. Alonso, R. Cimino, and K. Horn, Phy. Rev. Lett. **64**, 1947 (1990).
[52]S. Chang, I. M. Vitomirov, L. J. Brillson, D. F. Rioux, P. D. Kirchner, G. D. Pettit, J. M. Woodall, and M. H. Hecht, Phys. Rev. B **41**, 12 299 (1990).
[53]C. M. Aldao, G. D. Waddill, P. J. Benning, C. Capasso, and J. H. Weaver, Phys. Rev. B **41**, 6092 (1990).
[54]D. Mao, A. Kahn, M. Marsi, and G. Margaritondo, Phys. Rev. B **42**, 3328 (1990).
[55]X. Yin, H.-M. Chen, F. H. Pollak, Y. Chen, P. A. Montano, P. D. Kirchner, G. D. Pettit, and J. M. Woodall, Appl. Phys. Lett. **58**, 260 (1991).
[56]A. Y. Cho and P. D. Dernier, J. Appl. Phys. **49**, 3328 (1978).
[57]S. P. Svensson, G. Landgren, and T. G. Andersson, J. Appl. Phys. **54**, 4474 (1983).
[58]M. Missous, E. H. Rhoderick, and K. E. Singer, J. Appl. Phys. **60**, 2439 (1986).
[59]W. I. Wang, J. Vac. Sci. Technol. B **1**, 574 (1983).
[60]C. Barret and J. Massies, J. Vac. Sci. Technol. B **1**, 819 (1983).
[61]D. C. Sun, H. Sakaki, H. Ohuo, Y. Sekiguchi, and T. Tanoue, in *Stabilization of Schottky Barrier Properties of Single-Crystal Al/GaAs and Al/AlGaAs/GaAs Contacts Prepared by Molecular Beam Epitaxy,* Inst. Phys. Conf. Ser. No. 63 (IOP, Bristol, 1981), Chap. 7, p. 311.
[62]K. Okamoto, C. E. C. Wood, L. Rathbun, and L. F. Eastman, J. Appl. Phys. **53**, 4521 (1982).
[63]J. C. Costa, F. Williamson, T. J. Miller, K. Beyzavi, M. I. Nathan, D. S. L. Mui, S. Strite, and M. Morkoç, Appl. Phys. Lett. **58**, 382 (1991).
[64]G. D. Waddill, I. M. Vitomirov, C. M. Aldao, S. G. Anderson, C. Capasso, J. H. Weaver, and Z. Liliental-Weber, Phys. Rev. B **41**, 5293 (1990).
[65]J. R. Waldrop, J. Vac. Sci. Technol. B **2**, 445 (1984).
[66]K. L. I. Kobayashi, N. Watanabe, T. Narusawa, and H. Nakashima, J. Appl. Phys. **58**, 3758 (1985).
[67]R. Ludeke, T.-C. Chiang, and D. E. Eastman, J. Vac. Sci. Technol. **21**, 599 (1982).
[68]R. T. Tung, Phys. Rev. Lett. **52**, 561 (1984).
[69]J. M. Woodall, G. D. Pettit, T. N. Jackson, C. Lanza, K. L. Kavanagh, and J. M. Mayer, Phys. Rev. Lett. **51**, 1783 (1983).
[70]C. J. Palmstrøm, T. L. Cheeks, H. L. Gilchrist, J. G. Zhu, C. B. Carter, and R. E. Nahory, in *Schottky Barrier Height Control in Metal-III-I Epitaxy, Materials Research Society Extended Abstract (EA-21)* (MRS, Pittsburgh, 1990), p. 63.
[71]C. J. Spindt, M. Yamada, P. L. Meissner, K. Miyano, A. Herera, A. J. Arko, G. D. Pettit, and W. E. Spicer, J. Vac. Sci. Technol. B **9**, 2090 (1991).
[72]D. Mao, A. Kahn, G. LeLay, M. Marsi, G. Margaritondo, M. Santos, M. Shanyegan, L. T. Florez, and J. P. Harbison, J. Vac. Sci. Technol. B **9**, 2083 (1991).
[73]S. P. Wilks, J. J. Morris, D. A. Woolf, and R. H. Williams, J. Vac. Sci. Technol. B **9**, 2118 (1991).
[74]C. Mailhiot and C. B. Duke, Phys. Rev. B **33**, 1118 (1986).
[75]S. Chang, J. L. Shaw, R. E. Viturro, J. J. Brillson, P. D. Kirchner, and J. M. Woodall, J. Vac. Sci. Technol. A **8**, 3803 (1990).